Investigation on the role of nitrates in the microwave-assisted autoclave Pechini synthesis of aluminoborate phosphors

Jérémy Cathalan, Mathieu Salaün, Audrey Potdevin, François Réveret, Geneviève Chadeyron, Isabelle Gautier-Luneau

Journal of Materials Chemistry C

ROYAL SOCIETY OF CHEMISTRY

PAPER

Cite this: J. Mater. Chem. C, 2024, 12, 19603

Investigation on the role of nitrates in the microwave-assisted autoclave Pechini synthesis of aluminoborate phosphors†

Jérémy Cathalan,[ab] Mathieu Salaün, *[a] Audrey Potdevin, [b] François Réveret, [b] Geneviève Chadeyron [b] and Isabelle Gautier-Luneau *[a]

Received 4th June 2024,
Accepted 23rd October 2024

DOI: 10.1039/d4tc02300e

rsc.li/materials-c

Aluminoborate (AB) powder prepared by the Pechini method is a promising rare earth-free phosphor for white light emitting diodes applications. The photoluminescence emission is attributed to organic molecules, polycyclic aromatic hydrocarbons, trapped in the inorganic matrix. We discuss the replacement of the usual reflux heating of the Pechini synthesis by an autoclave microwave-assisted step. Morphological and structural properties seem not changed by the evolution of the heating method while the emission under UV and blue excitation (385–450 nm) are improved in terms of bandwidth and external quantum yield. The main difference between the reflux and the microwave-assisted autoclave heating is that the NO_x gases provided by aluminium nitrate precursor are not evacuated from the reactional medium with this latter. From this statement, the role of the nitrate in the precursors has been investigated. The optical, structural and thermal properties of aluminoborate powders with nitrate (^{15}N nitrogen labelling) or without nitrate are described. In particular, thanks to ^{15}N labelling, thermogravimetric analysis coupled to mass spectrometry and the study of the fluorescence decays suggest the presence of nitrogenous compounds in the composition of the polycyclic aromatic hydrocarbons emitting centres.

1. Introduction

Alternative rare-earth (RE)-free luminescent materials are attracting much attention in the phosphor converted-light emitting diodes (pc-LEDs) domain. Currently, these devices are typically constituted of a blue-chip source associated with one or several rare earth-containing phosphors. The yttrium aluminium garnet doped with trivalent cerium ion (YAG:Ce^{3+}) partially converts the blue emission of the chip into a yellow contribution.[1,2] Usually, a second phosphor emitting in the red domain is combined with YAG:Ce^{3+} to generate a warm white light. Nitrides or sulfides doped with the divalent europium ion have been widely used to this end.[3–5] Nevertheless, several new families of RE-free phosphors have been developed to reduce RE consumption. For example, a partial substitution of critical elements is implemented with the red phosphor composed of K_2SiF_6 matrix doped with the transition metal ion Mn^{4+}.[6] One of the main drawbacks of this phosphor is the use of hydrofluoric acid (HF) during synthesis. New HF-free methods are emerging, but problems remain with the stability of the Mn^{4+} oxidation state.[7] Other interesting options such as quantum dots (QDs), characterized by tuneable emission over the visible range and high quantum yield (QY), are possible new phosphors for pc-LEDs.[8,9] Unfortunately, the use of cadmium in the composition of the more efficient QDs has been limited by the legislation of the European Union restriction of hazardous substances (RoHS).[10] It is the reason why cadmium-free QDs have been recently developed but their performance remains a step below that of cadmium-based QDs.[11,12] Eventually, organic[13] and hybrid[14,15] phosphors are considered as potential interesting luminescent materials for pc-LEDs applications, but their stability under operating temperature and photonic stresses has been pointed out as insufficient.[13] Moreover, with the previous examples, it is still difficult to generate a broad neutral or warm white emission covering the entire visible spectrum with a single phosphor excited in the UV or blue wavelengths region. Finally, inorganic defect-related luminescent materials could be promising solutions. Different metal oxides as vanadate,[16] titanate,[17] zinc oxide,[18] or silicates[19,20] have been described in the literature as carbon defects- or oxygen vacancies-related luminescent materials, generating a wide emission band corresponding to cold-to-warm white light with possible application in LED devices. Ogi *et al.* reported their research into boron carbon oxynitride (BCNO) powders synthesised by

[a] Univ. Grenoble Alpes, CNRS, Grenoble INP, Institut Néel, Grenoble 38000, France. E-mail: mathieu.salaun@neel.cnrs.fr, Isabelle.Gautier-Luneau@neel.cnrs.fr
[b] Université Clermont Auvergne, Clermont Auvergne INP, CNRS, Institut de Chimie de Clermont-Ferrand, Clermont-Ferrand F-63000, France

† Electronic supplementary information (ESI) available. See DOI: https://doi.org/10.1039/d4tc02300e

solvothermal process and exhibiting a broad and tuneable luminescence.[21] The microwave heating route has also been used to prepare luminescent materials, such as BCNO characterized by a warm white photoluminescence (PL),[22] and promising for pc-LED phosphors application. Unfortunately, there is a lack of information on the chemical and photonic stability and the exact nature of the chemical species at the origin of the luminescence of most of the aforementioned hybrid phosphors.

An original approach, based on aluminoborate powders derived from the modified Pechini method, was developed several years ago. Initially, yttrium and zinc aluminoborates (YAB[23] and ZAB[24]) were studied before investigating simpler aluminoborate (AB)[25] luminescent powders. In the case of these aluminoborates (YAB, ZAB and AB), the photoluminescence emission results from carbon-based molecules trapped in the inorganic matrix. The presence of polycyclic aromatic hydrocarbons (PAHs) has been reported in the YAB phosphors.[26–28] These PAHs are associated with the use of citric acid and D-sorbitol respectively employed as complexing agents and polymeric precursors during the synthesis. The latter has been optimized in terms of precursors ratios and thermal treatments parameters in the AB synthesis, in order to broaden the emission in the warm wavelengths range.[25]

In this paper, we describe an original evolution of the Pechini synthetic protocol for which the usual reflux heating has been replaced by a microwave-assisted (MW) autoclave heating. Microwave-assisted synthesis are currently widely used in many fields, both in organic and inorganic chemistry.[29,30] They can be effectively applied to any reaction scheme with greater heating homogeneity, creating faster reactions, improving yields, and producing cleaner chemistries. In addition, microwave synthesis creates completely new possibilities in chemical transformations. Thanks to the specific nature of the microwave heating mechanism (dipole reaction or ionic conduction), microwaves can transfer energy directly to the reactive species, and can promote transformations that are not currently possible with conventional heating. Furthermore, the use of autoclaves enables a pressure/temperature pair to be applied according to the nature of the solution (solvent, volume, reagents), thereby accelerating the reaction kinetics. Optical properties improvement arising from the heating method modification are presented. As the phosphors obtained have different optical properties to those of samples derived from the Pechini reflux route, an investigation into the role of nitrates in the synthesis and production of luminescent powders was carried out. Hence, alternative nitrate-free aluminium precursor has been used to synthesise AB powders. Thermal analyses have been performed on new samples prepared with ^{15}N nitrogen labelling to better unravel the nature of luminescent species. The influence of nitrates on structural and morphological properties of powders has also been examined. Together with optical characterizations, these studies have allowed us to discuss the role of nitrates on the photoluminescence in the AB powders and to propose an example of a nitrogenous compound that could be responsible for luminescence in these materials.

2. Experimental

2.1. Materials

Citric acid monohydrate (Cit; purity 99.0+%) and nitric-^{15}N acid (98 atom% ^{15}N) were purchased from Sigma-Aldrich. Aluminium nitrate $Al(NO_3)_3\ 9H_2O$ (purity 99.0+%), aluminium lactate $Al(C_3H_5O_3)_3$ ($Al(Lact)_3$; purity 90–95%, 5% water), D-sorbitol (Sorb; purity 97.0+%), boric acid H_3BO_3 (purity 99.8%) and ultrapure water (0.63 μS cm^{-1}) were purchased from Fisher Scientific.

2.2. Synthesis of AB aluminoborate phosphors

The modified Pechini method usually employed to synthesise AB powder involves a 48-hour reflux heating during which the metals (aluminium and boron) are complexed by citric acid and sorbitol. The optimised parameters determined for the modified Pechini synthesis, namely, Al/B = 0.5, Cit/Sorb = 1, and (Cit + Sorb)/(Al + B) = 6.5 ratios, and reported in a previous study,[25] have been used for the synthesis of powders with microwave heating. First, 250 mL of an aqueous solution containing citric acid monohydrate (136.5 mmol), $Al(NO_3)_3\ 9H_2O$ (14 mmol), D-sorbitol (136.5 mmol) and H_3BO_3 (28 mmol) were divided into 8 equal volumes in 8 quartz autoclaves with a filling rate of 40% of the 80 mL maximum capacity. The microwave heating process consists in applying an initial power of 600 W until the solution temperature reaches 140 C (measured by IR detection) under vigorous stirring. Afterward, the power is modulated to keep this temperature stable. Under these conditions, pressure inside the autoclaves rises to 8 to 10 bar until the citric acid decarboxylation reaction which brings pressure up to 15 bar. After 90 minutes, the heating is stopped and the solution cools naturally to room temperature. The obtained resin is viscous and brown in colour. Fig. 1 presents all the process steps with the heat treatments parameters kept identical to the values previously optimized[25] leading to the AB_{MW_init} powder. Due to the specific heating process of MW compared to reflux heating, the synthesis conditions were again optimised to generate the broadest and warmest emission possible, associated with the highest possible external quantum yield (eQY). The synthesis parameters studied were chosen within the ranges 20 C h^{-1} heating rate (HR) 90 C h^{-1} and 680 C calcination temperature T_{ca} 720 C (Fig. S1, ESI†).

The AB_{MW} powder that best meets the desired criteria (namely, a powder with a broad emission spectrum covering the entire visible range under excitation from commercial UV and/or blue LEDs with the best optical performance) is the one synthesised under the following conditions: a HR = 30 C h^{-1} and a T_{ca} = 700 C. This AB_{MW} powder will be used for the studies presented in this paper.

AB_{MW_Lact} powders were prepared as AB_{MW} by replacing the $Al(NO_3)_3\ 9H_2O$ precursor with aluminium lactate $Al(Lact)_3$.

$AB_{MW\_Lact\_HNO_3}$ powders were prepared as AB_{MW_Lact} by adding 2.80 mL of nitric acid solution HNO_3 (68 wt%) leading to a (NO_3^-)/Al ratio equal to 3.

$AB_{MW\_Lact\_^{15}N}$ powders were prepared as AB_{MW_Lact} adding 2.80 mL of HNO_3 solution enriched with 98% of ^{15}N. The (NO_3^-)/Al ratio equal to 3.

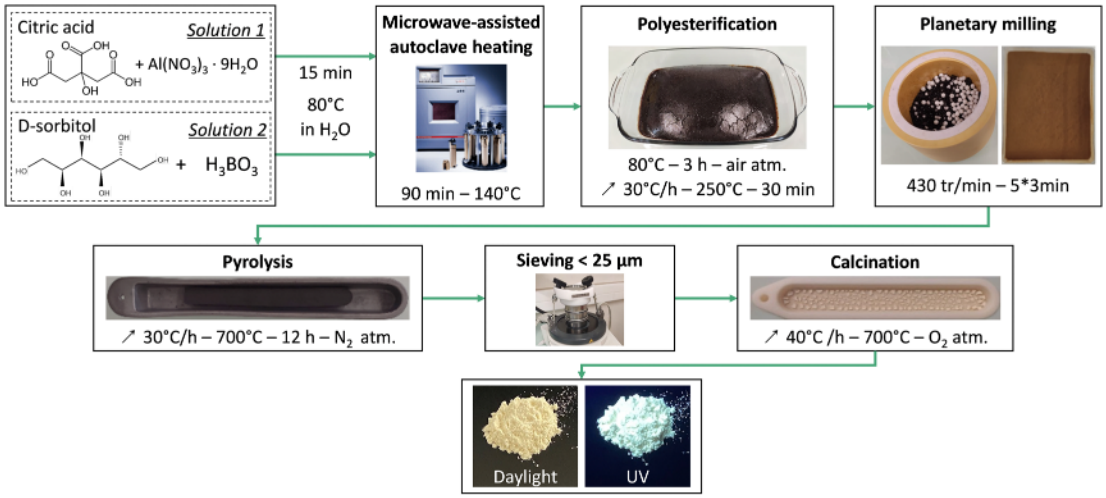

Fig. 1 Modified Pechini synthesis with heating method changed from reflux to microwave-assisted autoclave heating leading to AB_{MW_init}.

Note that the modified Pechini method with microwave heating compared to reflux heating leads to a substantial reduction in synthesis time from one week to five days.

2.3. Characterizations

Powder X-ray diffraction. PXRD patterns of AB powders were recorded using a Bruker D8 Endeavor diffractometer operating with Cu-K radiation (= 1.5418 Å) with a goniometer in a symmetrical geometry. The data were collected in a 2θ range between 10 and 60 with a scan speed of 1 per min and a step size of 0.033 per step.

Thermal analysis. Thermogravimetric analysis coupled mass spectrometry. Thermogravimetric analysis (TGA) was carried out with a symmetrical SETARAM TAG 16 equipment, using 30 mg samples within 100 µL alumina crucibles and a heating rate of 5 C per min under continuous oxygen flow (Airproducts, alphagaz 2). These thermal analyses were directly coupled to a HIDEN analytical apparatus (QGA-HAL201-RC) mass spectrometer (MS) to analyse the gaseous by-products of decompositions.

Granulometry. The grain size of the powders was measured by laser granulometry using a Malvern Mastersizer 2000. The dispersing agent was absolute ethanol.

Microscopy. The powder particles have been observed in a field emission scanning electron microscope (FESEM) Zeiss Ultra + operating at 2 kV and 4 kV.

Quantum yields & photoluminescence emission. QY efficiencies and emission spectra of the powders were measured using a C9920-02G PLQY integrating sphere measurement system from Hamamatsu Photonics. The setup consisted of a 150 W monochromatized Xe lamp, an integrating sphere (Spectralon coating, diameter = 3.3 in) and a high-sensitivity CCD camera. All measurements were carried out at room temperature. External quantum yield (eQY) was calculated from the internal quantum yield (iQY) and absorption coefficient (Abs) measurements according to eqn (1):

$$eQY = iQY \times Abs \quad (1)$$

Time-resolved photoluminescence (TRPL). TRPL was performed at room temperature. To study the fluorescence decays, a picosecond laser diode (375 nm) was used as an excitation source. The pulse duration was 65 ps and the repetition rate was 2 MHz. To study the phosphorescence decays, we used a nanosecond laser with a pulse duration and a repetition rate respectively equal to 5 ns and 10 Hz. For both measurements, the photoluminescence signal was focused on the slits on a 30 cm focal monochromator (FLS 980) coupled with a Hamamatsu photomultiplier.

3. Results and discussion

3.1. Evolution of the heating method in Pechini-synthesized AB powder

As mentioned in the introduction, the Pechini synthesis process includes a microwave heating step to replace the long reflux heating step used in our previous study[25] (see Fig. 1). In addition to save synthesis time, MW heating process gives access to different reaction kinetics to conventional heating. Hence, it seemed interesting to see the effect of microwave heating process on the properties of aluminoborate phosphors powders.

After the same pyrolysis/calcination process, the AB powder synthesised with the MW heating method (AB_{MW_init}) presents a broader and red-shifted emission compared to the reflux-heated one (AB_{reflux}) (Fig. S2, ESI†).

The evolution of the optical properties related to different heating modes led us to realize a new optimisation of calcination parameters, namely heating rate (HR) and calcination temperature (T_{ca}) (see experimental part). The powder that best fulfils the desired criteria is the one prepared with a HR = 30 C per h and a T_{ca} = 700 C, named AB_{MW} and will be considered for the studies presented in this paper. The optical performance, emission spectrum under 385 nm excitation, and eQY of this powder are compared to those of AB_{reflux} in Fig. 2. The excitation

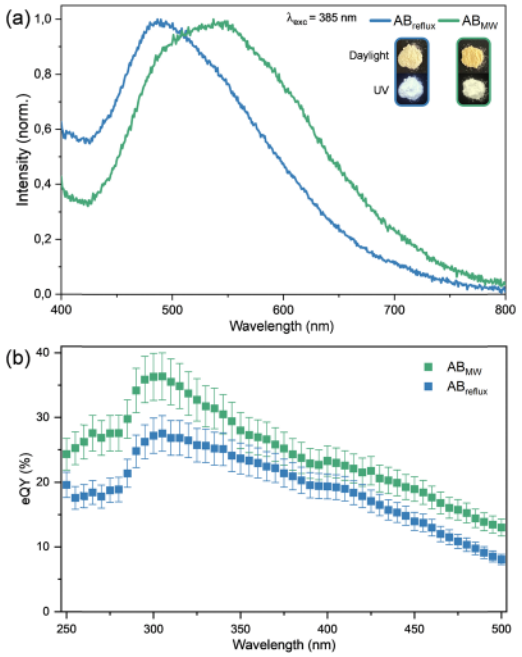

Fig. 2 (a) Normalized emission spectra of AB_{MW} and AB_{reflux} under 385 nm excitation with dashed lines corresponding to the emission wavelengths selected for the fluorescence decay measurements (b) associated eQY in the UV and blue areas (250–500 nm).

spectra and the trichromatic coordinates on the CIE diagram of both powders are presented in Fig. S3 and S4 (ESI†), respectively.

The emission spectrum is broadened by 40 nm and red-shifted by 60 nm, while the eQY is increased by 3 to 5% in the 385–450 nm range. Morphological and structural properties of the two luminescent powders are identical (Fig. S5, ESI†). Indeed, both XRD patterns show the $Al_4B_2O_9$ phase as well as a partial recrystallization of H_3BO_3, which proves that the optical changes result from factors other than structural and morphological features. Therefore, time-resolved photoluminescence (TRPL) measurements have been carried out on AB_{reflux} and AB_{MW}, under 400 nm excitation. The studied emission wavelengths are 450 nm, 500 nm and 560 nm, which correspond to different emission ranges of the samples, potentially related to different types of emitting centres. The fluorescence decays recorded on a 9 ns range and normalized are presented in Fig. 3. They can be fitted with a double-exponential curve (eqn (2)):

$$y = \quad \exp\left(\frac{-t}{\tau}\right) + \quad {}_2\exp\left(\frac{-t}{\tau_2}\right), \qquad (2)$$

In this equation, τ_1 and τ_2 are the short and long lifetimes and their weighting coefficients are A_1 and A_2 respectively. The results of fitting all the decays are gathered in Table 1. The two fitting lifetimes indicate that the emission is linked to the existence of several types/sizes of emitting centres in the powder. The evolution of the fitting parameters, especially the lifetimes, is similar for the two samples. Indeed, in both cases, the values of the short and long lifetimes increase with the emission wavelengths (Table 1). This result shows that the nature of the emitting centres is close between the two powders. Nevertheless, for each emission

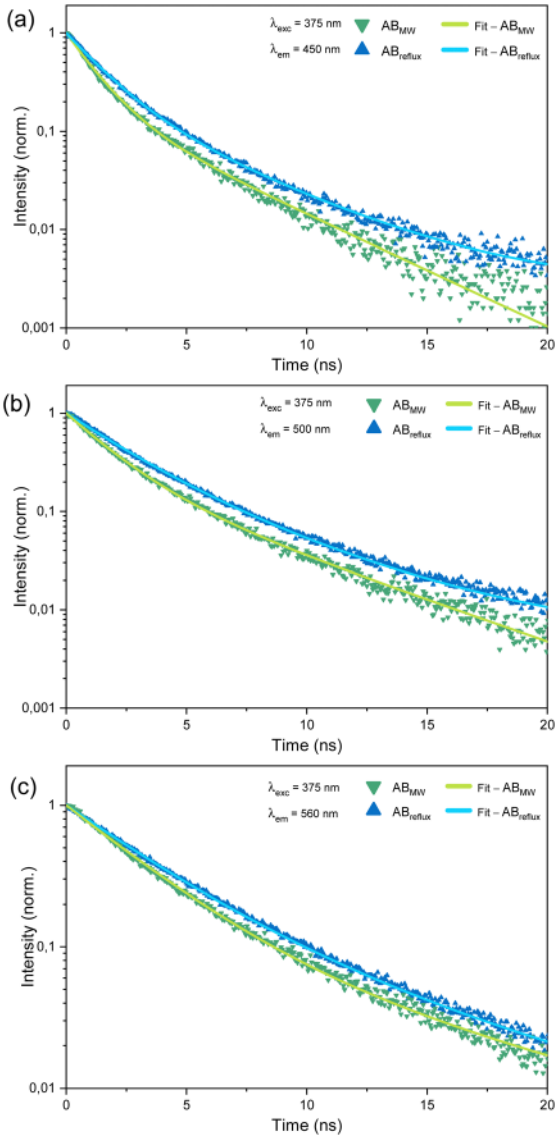

Fig. 3 Room temperature fluorescence decays of AB_{MW} and AB_{reflux} powders under 400 nm excitation and for three different emission wavelengths (a) $_{em}$ = 450 nm (b) $_{em}$ = 500 nm (c) $_{em}$ = 560 nm.

wavelength studied separately, as we can observe in Fig. 3, some variations can be pointed out between the AB_{reflux} and AB_{MW} decays. In particular, for the three emission wavelengths considered, both short and long lifetimes, τ_1 and τ_2 respectively, are

Table 1 Fit parameters obtained from the fluorescence decays of AB_{MW} and AB_{reflux} powders under 400 nm excitation for 450 nm, 500 nm and 560 nm emissions

Powder	$_{em}$ (nm)	τ_1 (ns)	τ_2 (ns)	A_1 (%)	A_2 (%)	R^2
AB_{MW}	450	1.1 ± 0.1	3.7 ± 0.1	80	20	0.9979
	500	1.6 ± 0.1	4.5 ± 0.1	69	31	0.9989
	560	2.3 ± 0.1	6.0 ± 0.1	66	34	0.9992
AB_{reflux}	450	1.4 ± 0.1	4 ± 0.1	76	24	0.9993
	500	2.3 ± 0.1	5.2 ± 0.1	73	27	0.9989
	560	3.3 ± 0.1	8 ± 0.1	80	20	0.9994

always shorter for AB_{MW} compared to AB_{reflux}. This evidences that the nature, size or environment of the emitting centres are different according to the heating method used during the Pechini synthesis of AB powders.

An important difference using an autoclave during synthesis is that the system remains closed whereas reflux heating allows gases to be vented through the column, in particular NO_x, associated with brownish fumes (Fig. S6, ESI†). To point out the impact of nitrates from the aluminium precursor on the luminescent powder properties, a nitrate-free synthesis has been carried out. Results obtained will be discussed in the following section.

Finally, in order to demonstrate the thermal stability of our powders, they were subjected to heat treatments at different temperatures, ranging from 55 C to 150 C, for durations between 16 and 160 hours. As illustrated in Fig. S7 (ESI†), no change in emission spectrum profile or intensity was observed, thus confirming the good stability of our compounds under thermal stress. A weak intensity decreasing is observed on the temperature-dependent emission spectra (Fig. S8, ESI†).

3.2. Investigation on the role of nitrates in the optical properties of AB powders

A nitrate-free precursor, aluminium lactate, has been used to replace aluminium nitrate in the synthesis of AB powder by the MW method.

Except for this new aluminium precursor, the same synthesis parameters were kept for the whole synthesis, including grain size distribution and heating treatments conditions. However interestingly differences have been observed during the synthesis with the aluminium lactate precursor: the pressure measured in the autoclave was lower (10 bar) compared to AB_{MW} (15 bar); the obtained brown solid after polyesterification step was less expanded and harder to grind (Fig. S9, ESI†). Indeed, the presence of nitrate ions, a powerful oxidizing agent, increases the pressure inside the autoclave through redox reactions with the citrate, leading to the formation of NO_x and the decarboxylation of the citrate. Various compounds are formed (such as acetonedicarboxylate and oxalate) in addition to the products formed by the decomposition of citric acid with temperature.[31,32]

After calcination at 700 C, the AB_{MW_Lact} powder obtained is white in colour and totally non-photoluminescent under 385 nm UV-radiation.

Thermogravimetric analysis of the pyrolyzed precursor (Fig. 4) reveals several differences between AB_{MW} and AB_{MW_Lact}. The total mass loss represents 84% and 70% for AB_{MW} and AB_{MW_Lact} respectively. Considering AB_{MW_Lact}, there is a delay of 50 C for the departures attributed to the water evaporation (100–200 C range) and the combustion of organic residues (450–600 C range) compared to AB_{MW}. Focusing on the 700 C zone (grey dashed frame, Fig. 4) related to the elimination of the emitting centres,[25] the mass loss is once again more important for AB_{MW} than AB_{MW_Lact} (3% *vs.* 1% – see zoom-in). This change in thermal behaviour leads to the hypothesis that all the emitting centres in AB_{MW_Lact} powder are already fully eliminated after calcination at 700 C. Powders synthesized from the aluminium lactate precursor and obtained after calcination at lower temperatures (580 C, 600 C and 620 C) produce a bluish photoluminescence under excitation at 385 nm, as shown in Fig. 5. By comparing the powders' PL, it is clear that the spectral coverage of AB_{MW_lact} is lower than that obtained for AB_{MW}. The eQYs at this excitation wavelength are respectively 5.8%, 8.8% and 6.2%, compared to 23.8% for AB_{MW}. These results prove that a weakly luminescent AB powder can be obtained from a nitrate-free aluminium precursor at lower temperatures. Thus, the brown solid obtained after the polyesterification step being less expanded and more difficult to grind, probably leads to an inorganic matrix which polymerizes more quickly, keeping less trapped organic moieties. This change in luminescence between powders with and without nitrates confirms the assumption that the emitting centers trapped in the matrix are of a different nature. To further understand these

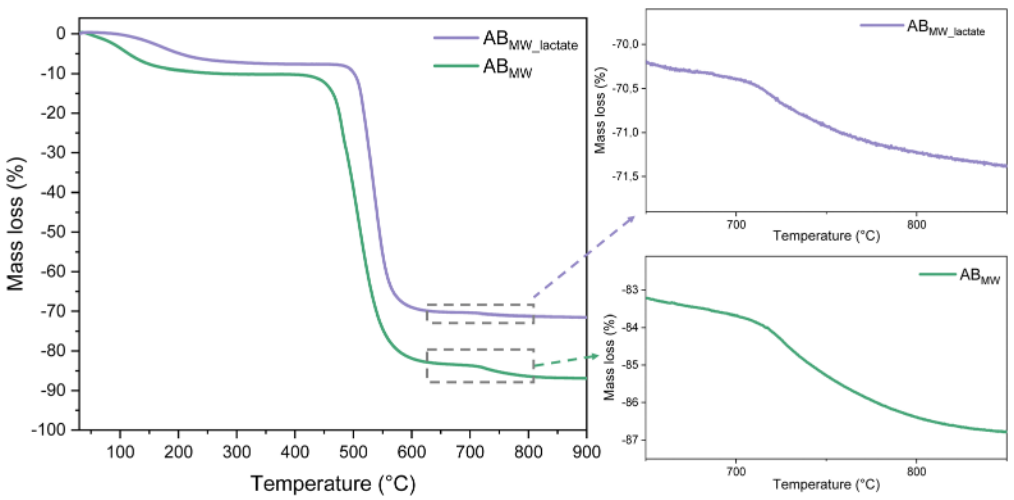

Fig. 4 Thermogravimetric analysis of AB_{MW} and AB_{MW_Lact} pyrolyzed powders under O_2 atmosphere corresponding to calcination conditions with dashed zones on the mass loss around 700 C corresponding to the elimination of emitting centres.

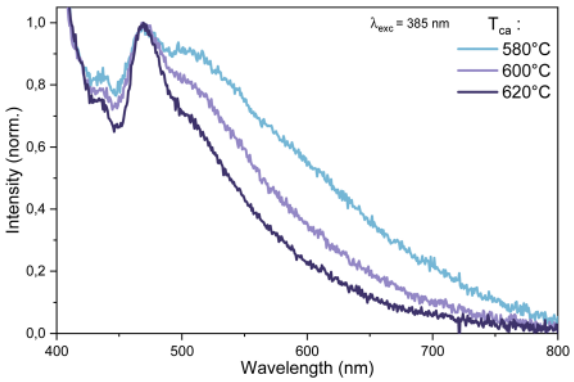

Fig. 5 Normalized room-temperature emission spectra of AB_{MW_Lact} powders calcined at 580 C, 600 C and 700 C under 385 nm excitation.

emission properties, fluorescence decays were recorded under 375 nm excitation for both types of sample.

Fig. 6 presents the fluorescence decay curves of aluminium nitrate (T_{ca} = 700 C) and lactate (T_{ca} = 600 C)-derived AB powders for the three same emission wavelengths studied for the AB_{reflux}/AB_{MW} comparison (450 nm, 500 nm and 560 nm) (Fig. 3). The TRPL measurements are described by exponential decays, for which the fitting parameters are gathered in Table 2. The corresponding equation for the double-exponential decays are identical to eqn (2), and a third term is added for the triple-exponential decay (eqn (3)):

$$y = \quad \exp\left(\frac{-t}{\tau}\right) + \quad {}_2 \exp\left(\frac{-t}{\tau_2}\right) + \quad {}_3 \exp\left(\frac{-t}{\tau_3}\right) \qquad (3)$$

The fluorescence decay profiles are quite similar for the 450 nm (Fig. 6a), with a higher value for the long lifetime (τ_2) of AB_{MW_Lact} than AB_{MW}. This behaviour is amplified for the 500 nm emission, in addition to a larger weight coefficient (A_2) for the AB_{MW_Lact} sample. Finally, at the emission wavelength of 560 nm, the response of the two powders is very different. Firstly, the short lifetime is much higher for AB_{MW} (τ_1 = 2.3 ns *vs.* 0.7 ns). Secondly, only AB_{MW_Lact} is characterised by a model with tri-exponential decay. Indeed, a third term corresponding to a longer lifetime (τ_3 = 12.4 ns) is needed to fine-tune the decay. This significant gap between the fluorescence decays of powders prepared with and without nitrate in the precursors demonstrates that the emission centres of AB_{MW} and AB_{MW_Lact} are, without doubt, different.

Table 2 Fit parameters obtained from the fluorescence decays of AB_{MW} and AB_{MW_Lact} powders under 375 nm excitation for 450 nm, 500 nm and 560 nm emissions

Powder	λ_{em} (nm)	τ_1 (ns)	τ_2 (ns)	τ_3 (ns)	A_1 (%)	A_2 (%)	A_3 (%)	R^2
AB_{MW}	450	1.1 ± 0.1	3.7 ± 0.1		80	20		0.9979
	500	1.6 ± 0.1	4.5 ± 0.1		69	31		0.9989
	560	2.3 ± 0.1	6.0 ± 0.1		66	34		0.9992
AB_{MW_Lact}	450	1.2 ± 0.1	4.6 ± 0.1		80	20		0.9986
	500	1.4 ± 0.1	5.7 ± 0.1		55	45		0.9985
	560	0.7 ± 0.1	5.0 ± 0.1	12.4 ± 0.1	49	45	6	0.9976

Although the calcination temperatures are different, it appears that the luminescence are of a dissimilar nature, particularly in that AB_{MW_lact} powders show a blue phosphorescence to the naked eye, unlike AB_{MW} powders. The luminescence decays of this signal were measured for both types of powder and are shown in Fig. S10 (ESI†) whereas the corresponding fitting parameters are gathered in Table S1 (ESI†). The intensity of the phosphorescence signal is approximately 40 times stronger for $AB_{MW\text{-}lact}$ than for AB_{MW}. Its origin has not yet been explained but it shows that nitrates play an undeniable role in the formation and trapping mechanisms, as well as in the nature of the emitting centres.

To determine if this behaviour can also be related to changes in the structural and morphological properties of these samples synthesised in the presence of lactate, these features were studied and are presented in the following section.

3.3. Influence of nitrates in the structural and morphological properties of AB powders

Fig. 7 shows the SEM images and XRD patterns recorded for the aforementioned calcined powders. AB_{MW_Lact} with T_{ca} = 600 C (luminescent) does not present any surface crystallisation (Fig. 7a and d), while on the same sample calcined at 700 C (non-luminescent), surface nanowires are visible in the SEM images (Fig. 7e). These nanowires are also observable on the luminescent AB_{MW} sample (Fig. 7f), attributed to the $Al_4B_2O_9$ phase by XRD (Fig. 7g) and characterized by HTEM (Fig. S11, ESI†). The nanometric size of the diffracting volumes is

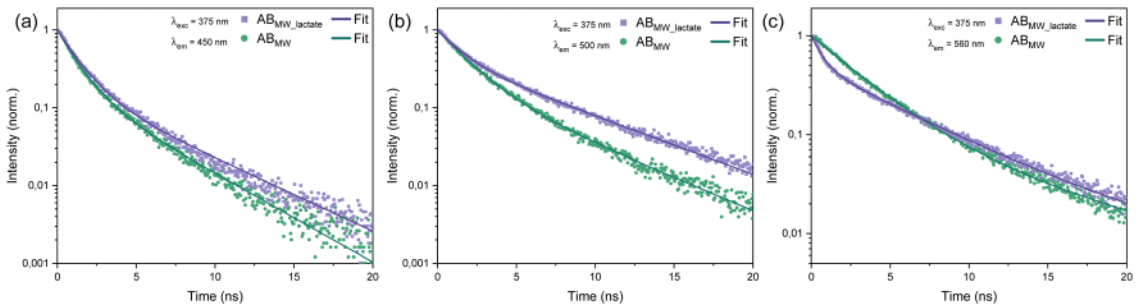

Fig. 6 Room temperature fluorescence decays of AB_{MW} and AB_{MW_Lact} powders under 375 nm excitation and for three different emission wavelengths (a) $_{em}$ = 450 nm (b) $_{em}$ = 500 nm (c) $_{em}$ = 560 nm.

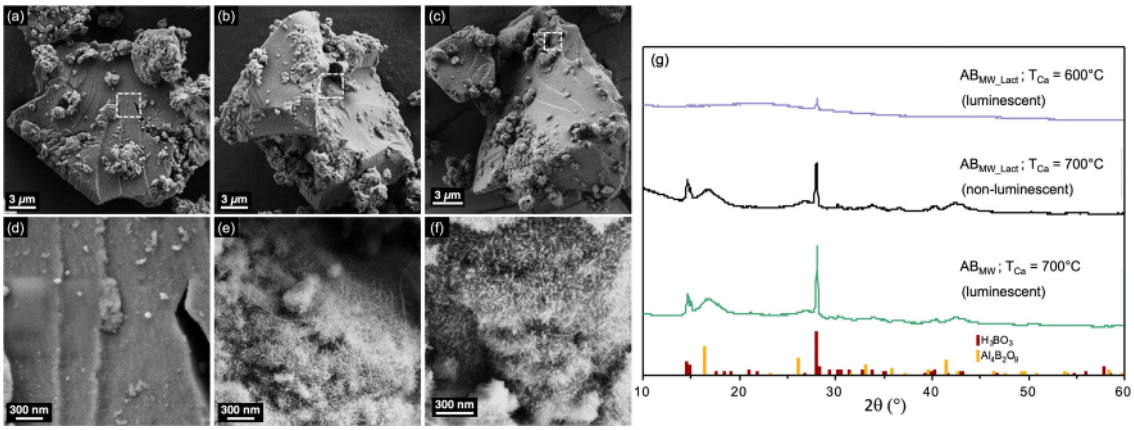

Fig. 7 SEM images of (a) and (d) AB_{MW_Lact} T_{ca} = 600 C (b) and (e) AB_{MW_Lact} T_{ca} = 700 C (c) and (f) AB_{MW} and (g) corresponding XRD patterns.

responsible for the broadness of the XRD peaks. For the three powders, H_3BO_3 recrystallization is also evidenced by the thin and intense XRD peak at 28 (Fig. 7g). The luminescence characteristics of aluminoborate powders do not therefore seem to be linked to these structural and morphological properties. Moreover, the chemical composition (Al, B, O) of the amorphous particles is homogeneous, as seen on the EDS maps (Fig. S11, ESI†). Indeed, whereas AB_{MW_Lact} (T_{ca} = 700 C) and AB_{MW} (T_{ca} = 700 C) are characterized by similar XRD patterns Fig. 7g) and morphologies, only the latter is luminescent. On the other hand, AB_{MW_Lact} (T_{ca} = 600 C) is luminescent, even though it does not contain the $Al_4B_2O_9$ phase and tends to trap less organic moieties. The optical properties of AB powders thus seem to be more closely linked to the presence or absence of nitrate or nitrogen in the emitting centres.

Nevertheless, at this point, it is not clear whether the changes in the optical properties are caused by the use of lactate itself or by the lack of nitrate. To clarify this, another sample named "$AB_{MW\_Lact+HNO_3}$" was prepared in which aluminium lactate was used as the aluminium precursor, and a quantity of HNO_3 corresponding to stoichiometric proportions

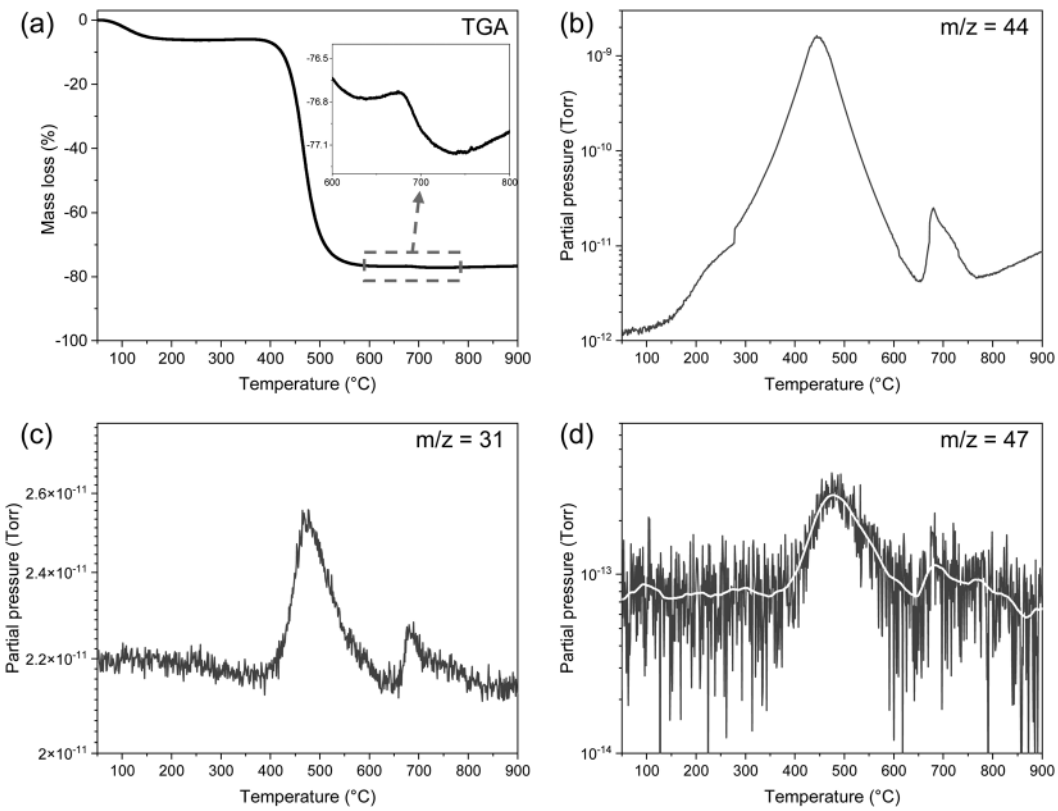

Fig. 8 Thermogravimetric analysis coupled with mass spectrometry of $AB_{MW\_Lact\_^{15}N}$ (a) TGA graph (b) CO_2 m/z = 44 (c) ^{15}NO m/z = 31 (d) $^{15}NO_2$ m/z = 47.

of $(NO_3)^-$, identical to that used for the synthesis of AB_{MW} (Table S2, ESI†), was added. Following the usual protocol, with T_{ca} = 700 C, the calcined powder $AB_{MW\_Lact+HNO_3}$ exhibits a photoluminescence emission profile similar to AB_{MW} (see Fig. S12, ESI†). This result confirms that the differences in optical properties between AB_{MW} and AB_{MW_Lact} stems from the presence or lack of nitrates in the precursors. Nitrate ions have a decisive influence on the optical properties of AB powders. The following characterisations aim to shed light on this role.

3.4. Identification of nitrogenous compounds as possible emitting centres

The presence of nitrogen atoms in the organic molecules (PAH) composing the emitting centres trapped in the inorganic matrix has been investigated. The TGA-MS analysis (Fig. 8) was carried out on a $AB_{MW\_Lact\_^{15}N}$ powder prepared with the same composition as $AB_{MW\_Lact+HNO_3}$ using a solution of nitric acid enriched with 98% of ^{15}N. This isotopic nitrogen enables to unambiguously follow the gaseous departures of ^{15}NO (m/z = 31) and $^{15}NO_2$ (m/z = 47), as the m/z values are different from the M + 2 isotopes of CO ($C^{18}O$: m/z = 30) and CO_2 ($C^{18}O_2$: m/z = 46), unlike ^{14}NO and $^{14}NO_2$ gases. The conditions are similar to the calcination treatment, under O_2 atmosphere. In Fig. 8a, the thermogram shows a mass loss of 0.3% around 700 C (see the insert), correlated to the elimination of the organic emitting centres. Indeed, after the first m/z = 44 (CO_2) departure related to the combustion of the organic precursors between 400 C and 500 C, a second elimination of CO_2 is underlined by the much weaker mass loss between 650 C and 750 C (Fig. 8b).

On both Fig. 8c and d, focused on ^{15}NO and $^{15}NO_2$ respectively, after the first departures between 400 C and 500 C, weaker departures between 650 C and 750 C are also observed. It demonstrates that the organic emitting centres of $AB_{MW\_Lact\_^{15}N}$, similar to AB_{MW} powders, contain nitrogen atoms in their composition. As there is no nitrogen in the precursors of AB_{MW_Lact}, this also corroborates the previous result, obtained with the analysis of the fluorescence decays, evidencing that the emitting centres of AB_{MW} and AB_{MW_Lact} are of different natures.

A previous study led on YAB phosphors, for which the photoluminescence origin is similar to AB,[33] proposed a possible hydroxyl functionalisation of the aromatic rings of the PAH thanks to DFT calculations. Here, we suggest that this functionalisation could also be nitrogen-based, as illustrated in Fig. 9.

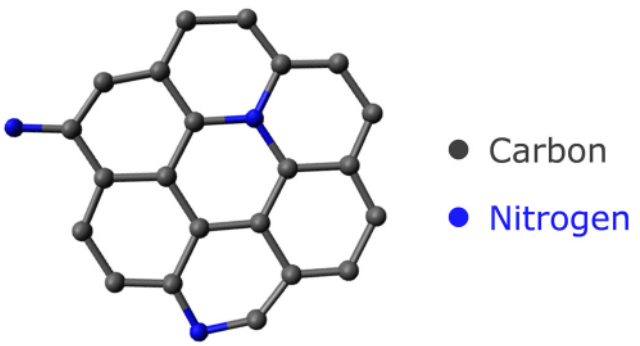

Fig. 9 Example of some possible positions of nitrogenous compounds in a PAH molecule, that may correspond to the emitting centres of AB_{MW}.

4. Conclusions

An enhancement in the Pechini synthesis of photoluminescent AB powders was accomplished by employing microwave-assisted autoclave heating as an alternative to traditional reflux heating. This innovative approach reduces the overall synthesis duration from seven to five days. The optimized calcination parameters were determined as HR = 30 C per h and T_{ca} = 700 C. Under these conditions, with UV excitation at 385 nm, the emission band is broader than with reflux heating, covering the entire visible spectrum from 400 nm to 700 nm. The powder demonstrates excitation compatibility with both UV and blue LEDs sources, reaching a peak external quantum yield (eQY) of 36% under excitation at 305 nm. The differences in optical properties, attributed to the switch from the open synthesis system to a closed system, retaining NO_x off-gas in solution, prompted an exploration of the influence of nitrate ions originating from the aluminium precursor. Aluminum nitrate was first replaced with aluminum lactate to perform a nitrate-free study. Then, ^{15}N labelled nitric acid was added to the synthesis with aluminium lactate with the same stoichiometry as the aluminium nitrate precursor. This study highlighted the dual role played by nitrate ions. Their oxidizing capacity allows on the one hand a better expansion of the brown solid after the polyesterification step (before thermal treatments), subsequently trapping more organic matter transformed into luminescent centres. On the other hand, thermogravimetric analysis coupled with mass spectrometry revealed nitrogenous compounds as emitting centres, contributing to the broad photoluminescence band observed in ABMW powders. The study of fluorescence decays of AB powders prepared with and without nitrates in the aluminium precursors has shown significantly different behaviours, supporting the assumption of nitrogenous compounds as main emitting centres in AB_{MW} powders. Possible molecules have been proposed. This progress in understanding the origin of photoluminescence in this aluminoborate powder holds the potential to enhance its optical properties, positioning this luminescent material as a promising candidate for rare earth-free phosphors. The phosphors obtained will not be able to meet the requirements of consumer lighting, but their optical performance, in terms of eQY, under commercial blue or UV LED excitation, is perfectly compatible with display or anti-counterfeiting marking applications.

Author contributions

Jérémy Cathalan: investigation, visualization, writting – orginal draft. Mathieu Salaün: funding acquisition, conceptualization, supervision, investigation, visualization and writting – review & editing. Audrey Potdevin: funding acquisition, conceptualization, supervision, investigation, visualization and writting – review & editing. François Réveret: formal analysis, investigation, visualization, writting – review & editing. Geneviève Chadeyron:

funding acquisition, conceptualization, supervision, investigation, project administration, visualization and writting – review & editing. Isabelle Gautier-Luneau: funding acquisition, conceptualization, supervision, investigation, project administration, visualization and writting – review & editing.

Data availability

The datasets supporting this article have been uploaded as part of the ESI.†

Conflicts of interest

There are no conflicts to declare.

Acknowledgements

The authors acknowledge Région Auvergne Rhône Alpes for its financial support in the frame of Pack Ambition Recherche 2019, ''LUMINOLED'' project.

Notes and references

1 N. U. Islam, M. Usman, S. Rasheed and T. Jamil, *ECS J. Solid State Sci. Technol.*, 2021, **10**, 106004.
2 A. C. Berends, M. A. van de Haar and M. R. Krames, *Chem. Rev.*, 2020, **120**, 13461–13479.
3 K. Uheda, N. Hirosaki, Y. Yamamoto, A. Naito, T. Nakajima and H. Yamamoto, *Electrochem. Solid-State Lett.*, 2006, **9**, 22–25.
4 K. N. Kim, J.-M. Kim, K. J. Choi, J. K. Park and C. H. Kim, *J. Am. Ceram. Soc.*, 2006, **89**, 3413–3416.
5 P. F. Smet, A. B. Parmentier and D. Poelman, *J. Electrochem. Soc.*, 2011, **158**, R37.
6 T. Takahashi and S. Adachi, *J. Electrochem. Soc.*, 2008, **155**, E183.
7 L. Huang, Y. Zhu, X. Zhang, R. Zou, F. Pan, J. Wang and M. Wu, *Chem. Mater.*, 2016, **28**, 1495–1502.
8 H. Shen, Q. Gao, Y. Zhang, Y. Lin, Q. Lin, Z. Li, L. Chen, Z. Zeng, X. Li, Y. Jia, S. Wang, Z. Du, L. S. Li and Z. Zhang, *Nat. Photonics*, 2019, **13**, 192–197.
9 S. Sadeghi, B. Ganesh Kumar, R. Melikov, M. Mohammadi Aria, H. Bahmani Jalali and S. Nizamoglu, *Optica*, 2018, **5**, 793.
10 The European Parliament and the Council of the and European Union, RoHS Directive, **https://ec.europa.eu/environment/topics/waste-and-recycling/rohs-directive_en**, (accessed May 11, 2022).
11 R. Valleix, Q. Zhang, D. Boyer, P. Boutinaud, G. Chadeyron, Y. Feng, H. Okuno, F. Réveret, H. Hintze-Bruening and F. Leroux, *Adv. Mater.*, 2021, **33**, 2103411.
12 X. Zhou, J. Ren, W. Cao, A. Meijerink and Y. Wang, *Adv. Opt. Mater.*, 2023, **11**, 2202128.
13 R. Boonsin, G. Chadeyron, J.-P. Roblin, D. Boyer and R. Mahiou, *J. Mater. Chem. C*, 2015, **3**, 9580–9587.
14 W. Liu, D. Banerjee, F. Lin and J. Li, *J. Mater. Chem. C*, 2019, **7**, 1484–1490.
15 X. Zhang, W. Liu, G. Z. Wei, D. Banerjee, Z. Hu and J. Li, *J. Am. Chem. Soc.*, 2014, **136**, 14230–14236.
16 L. K. Bharat, S.-K. Jeon, K. G. Krishna and J. S. Yu, *Sci. Rep.*, 2017, **7**, 42348.
17 A. E. Souza, R. A. Silva, G. T. A. Santos, M. L. Moreira, D. P. Volanti, S. R. Teixeira and E. Longo, *Chem. Phys. Lett.*, 2010, 3.
18 Y. Zhang, T. Gard, C. Theron, A. Apostoluk, K. Masenelli-Varlot, B. Canut, S. Daniele and B. Masenelli, *Appl. Surf. Sci.*, 2021, **540**, 148343.
19 W. H. Green, *Science*, 1997, **276**, 1826–1828.
20 G.-L. Davies, J. E. McCarthy, A. Rakovich and Y. K. Gun'ko, *J. Mater. Chem.*, 2012, **22**, 7358.
21 T. Ogi, Y. Kaihatsu, F. Iskandar, W.-N. Wang and K. Okuyama, *Adv. Mater.*, 2008, **20**, 3235–3238.
22 Y.-F. Yang, J.-J. Chen, Z.-Y. Mao, G.-H. Li, J. Xu, D.-J. Wang and B. D. Fahlman, *Acta Metall. Sin. (Engl. Lett.)*, 2017, **30**, 113–119.
23 V. F. Guimarães, L. J. Q. Maia, I. Gautier-Luneau, C. Bouchard, A. C. Hernandes, F. Thomas, A. Ferrier, B. Viana and A. Ibanez, *J. Mater. Chem. C*, 2015, **3**, 5795–5802.
24 P. Gaffuri, M. Salaün, I. Gautier-Luneau, G. Chadeyron, A. Potdevin, L. Rapenne, E. Appert, V. Consonni and A. Ibanez, *J. Mater. Chem. C*, 2020, **8**, 11839–11849.
25 J. Cathalan, M. Salaün, P. Gaffuri, A. Potdevin, F. Réveret, A. Ibanez, G. Chadeyron and I. Gautier-Luneau, *J. Mater. Sci.*, 2022, **57**, 15829–15842.
26 P. Burner, A. D. Sontakke, M. Salaün, M. Bardet, J. M. Mouesca, S. Gambarelli, A. L. Barra, A. Ferrier, B. Viana, A. Ibanez, V. Maurel and I. Gautier-Luneau, *Angew. Chem., Int. Ed.*, 2017, **56**, 13995–13998.
27 A. D. Sontakke, A. Ferrier, P. Burner, V. F. Guimarães, M. Salaün, V. Maurel, I. Gautier-Luneau, A. Ibanez and B. Viana, *J. Phys. Chem. Lett.*, 2017, **8**, 4735–4739.
28 M. Salaün, A. D. Sontakke, V. Maurel, J. M. Mouesca, A. L. Barra, V. F. Guimaraes, V. Montouillout, B. Viana, I. Gautier-Luneau and A. Ibanez, *MRS Bull.*, 2022, **47**, 1–12.
29 B. L. Hayes, *Microwave Synthesis: Chemistry at the Speed of Light*, CEM Pub., 2002.
30 A. Mirzaei and G. Neri, *Sens. Actuators, B*, 2016, **237**, 749–775.
31 M. M. Barbooti and D. A. Al-Sammerrai, *Thermochim. Acta*, 1986, **98**, 119–126.
32 R. Lopez-Garcia, *Kirk-Othmer Encyclopedia of Chemical Technology*, 2010, pp. 1–25.
33 M. Salaün, A. D. Sontakke, V. Maurel, J. M. Mouesca, A. L. Barra, V. F. Guimaraes, V. Montouillout, B. Viana, I. Gautier-Luneau and A. Ibanez, *MRS Bull.*, 2022, **47**, 231–242.